Smart Mater. Struct. **8** (1999) 365–379. Printed in the UK PII: S0964-1726(99)02176-X

Design of smart composite materials using topology optimization

O Sigmund† and S Torquato‡

† Department of Solid Mechanics, Technical University of Denmark, DK-2800 Lyngby, Denmark
‡ Department of Civil Engineering and Operations Research and Princeton Materials Institute, Princeton University, Princeton, NJ 08544, USA

Received 2 December 1997, in final form 2 November 1998

Abstract. The topology optimization method is used to find the distribution of material phases that extremizes an objective function (e.g., thermal expansion coefficient, piezoelectric coefficients etc) subject to constraints, such as elastic symmetry and volume fractions of the constituent phases, within a periodic base cell. The effective properties of the material structures are found using a numerical homogenization method based on a finite-element discretization of the base cell. The optimization problem is solved using sequential linear programming. We review the topology optimization procedure as a tool for smart materials design and discuss in detail two recent applications of it to design composites with extreme thermal expansion coefficients and piezocomposites with optimal hydrophone characteristics.

1. Introduction

Smart material systems often consist of mixtures of several different passive and active materials. Mixing the constituent materials in the right way makes it possible to make new smart composites with properties beyond those of the individual constituents. Whereas the modeling of composite materials consisting of various passive and active materials has been studied in detail in numerous research papers, only a few papers have considered the systematic design or synthesis of smart materials.

A promising new method for the systematic design of smart materials is the *topology optimization method*. The topology optimization method was founded a decade ago by Bendsøe and Kikuchi [1] and was originally intended for the design of mechanical structures. Since then, the method has reached a level of maturity where it is being applied to many industrial problems. In academia it is being used not only to solve structural problems but also in smart and passive material design, mechanism design, microelectromechanical systems (MEMS) design and many other design problems. In the following we will introduce the topology optimization in further detail, review its applications and discuss its applicability to smart materials design.

The basic form of a topology optimization problem can be defined as follows: *distribute a given amount of material in a design domain such that an objective function is extremized*. A typical example would be the design of a load-bearing structure for maximum stiffness (or minimum compliance) where the weight should be kept under a certain limit. Finding the optimal topology corresponds to finding the optimal connectedness, shape and number of holes in the structure such that the objective function is extremized.

The topology optimization problem is initialized by discretizing the design domain by a large number of elements. Allowing each element to be either solid or void, one can imagine that a 'bit-map' of the structure can be obtained by turning on or off the individual elements or pixels. This 0/1 problem is ill posed since a refinement of the mesh results in a solution with finer details [2]. In fact, it can be shown that optimal structures (at least for compliance optimization) will consist of regions with infinitely fine microstructure (e.g. [3] and references therein). In order to encompass composites, i.e. structures with fine microstructure, [1] introduced a microscale through the use of the so-called *homogenization approach to topology optimization*. For an overview of the homogenization approach to topology optimization and its mathematical background, the reader is referred to [4] and references therein. Recently the method has been applied to three-dimensional problems (e.g. [5, 6, 7]) and for multiple material problems [8]. A disadvantage of the homogenization approach is that it often produces structures with large 'grey' regions consisting of perforated material. This problem can be overcome by introducing a penalization of intermediate densities.

An alternative to the homogenization approach is the SIMP (simple isotropic material with penalization [9]) approach (see also [10, 11]). Using the SIMP approach the stiffness tensor of an intermediate density material is $C_{ijkl}(\rho) = C^0_{ijkl}\rho^p$, where C^0_{ijkl} is the stiffness tensor of solid material and p is the penalization factor which ensures that the continuous design variables are forced towards a black and white (0/1) solution. The influence of the penalty parameter can be explained as follows. By specifying a value of p higher than one, the local stiffness for $\rho < 1$ is lowered, thus making it 'uneconomical' to have intermediate densities in the optimal design. Even though the SIMP formulation is

0964-1726/99/030365+15$19.50

ill posed (mesh dependent), it is popular because it is easy to implement in commercial finite element codes and because the simple model allows for consideration of more advanced problems than the compliance optimization problem. A way of achieving well posedness of the SIMP problem is by restricting the design space by introducing a constraint on the density variation of the microstructure. This can be done by introducing a perimeter constraint [12, 13, 14, 15, 16], a local gradient constraint [17] or a (heuristic) filtering approach [18, 19].

In recent work, the SIMP approach to topology optimization has been applied to three-dimensional problems (e.g. [20, 21]), non-linear elasticity [22], plasticity [23, 24], stress constraints [25, 26], controlled structures [27] and in MEMS design [28, 29, 19]. It should be emphasized here that the references we have listed here by no means give an exhaustive listing of the numerous interesting applications of the topology optimization method which have appeared during recent years. For more references the reader is referred to the conference literature and to [4].

An application of the topology optimization method of special importance to smart materials design is the design of materials with extreme elastic properties. In this class of topology optimization problems, the design domain is the base cell of a periodic material and the objective function is to extremize some function of the effective properties. The design of material structures with extreme *elastic* properties is considered in [30, 18, 31, 32, 24], with extreme *thermoelastic* properties and three material phases in [18, 33, 34] and applications to design of *piezoelectric* composites are found for two-dimensional problems in [35] and for three dimensions in [21].

In this paper, we will review the topology optimization method applied to smart composite material design based on references [33, 34, 21].

The topology optimization procedure described here essentially follows the steps of conventional topology optimization procedures based on the SIMP approach. The design problem is initialized by defining a design domain (the base cell) discretized by a number of finite elements. The optimization procedure then consists in solving a sequence of finite-element problems followed by changes in density and/or material type of each of the finite elements, dependent on the local strain energies. For simple compliance optimization, this corresponds to adding material where the strain energy density is high and removing material where the strain energy density is low.

At each step of the topology optimization procedure, we have to determine the effective properties of the microstructure. There exist several methods to determine these properties. However, because the topology optimization method is based on finite-element discretizations, and because the finite-element method allows easy derivation and evaluation of the sensitivities of the effective properties with respect to design changes, we have chosen to use a finite-element based numerical homogenization procedure as developed in [36, 37].

We can use the topology procedure to design composite materials with extreme elastic, thermal or piezoelectric properties. In the case of elastic properties, for example, one can design materials that minimize the Poisson's ratio and hence create materials that possess the unusual property of having a negative Poisson's ratio [29]. Thermal applications include designing materials with negative thermal expansion coefficient or materials that could be used as thermal actuators. In the case of piezoelectricity, actuators that maximize the delivered force or displacement can be designed. Moreover, one can design piezocomposites that maximize the sensitivity to acoustic fields.

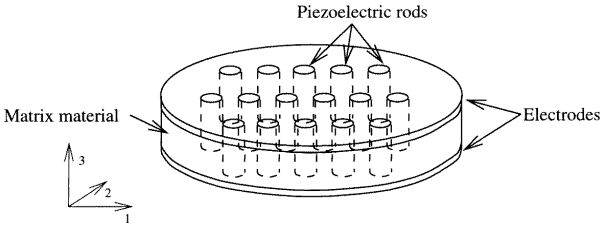

Figure 1. Sketch of the 1–3 piezocomposite construction.

We will describe the general topology optimization procedure applied to two- and three-phase designs, and concentrate on two recent applications of ours to design composites with extreme thermal expansion coefficients and piezocomposites with optimal hydrophone characteristics.

Materials with extreme or unusual thermal expansion behavior are of interest from both a technological and fundamental standpoint. Zero-thermal-expansion materials are needed in structures subject to temperature changes such as space structures, bridges and piping systems. Materials with large thermal displacement or force can be employed as 'thermal' actuators. A fastener made of a negative thermal expansion material, upon heating, can be inserted easily into a hole. Upon cooling, it will expand, fitting tightly into the hole.

A negative thermal expansion material has the counterintuitive property of contracting upon heating. Existing materials with negative expansions include glasses in the titania–silica family [38] at room temperature T, silicon and germanium [39] at very low T (< 100 K), and ZrW_2O_8 for a wide range of T [40]. Materials with *directional* negative expansion coefficients at room temperature include Kevlar, carbon fibers, plastically deformed (anisotropic) Invar (Fe–Ni alloys) [41] and certain molecular networks [42].

Piezoelectric transducers have been employed as sensors and transmitters of acoustic signals in ultrasound medical imaging, non-destructive testing and underwater acoustics [43, 44]. Here we consider a class of composite piezoelectric transducers for hydrophone applications: 1–3 composites consisting of an array of parallel piezoceramic rods embedded in a polymer matrix with electrode layers on the top and bottom surfaces (see figure 1).

The anisotropic piezoelectric response of pure PZT under pure hydrostatic loading is such that it has poor hydrophone performance characteristics. Specifically, consider a PZT rod poled in the axial direction (x_3-direction) subjected to hydrostatic load. The induced polarization field in the axial direction is found to be proportional to the applied pressure, i.e.,

$$D_3 = d_h^{(*)}\, T \qquad d_h^{(*)} = d_{33}^{(*)} + 2d_{13}^{(*)} \tag{1}$$

where D_3 is the dielectric displacement in the x_3-direction, T is the amplitude of the applied pressure, $d_h^{(*)}$ is the hydrostatic coupling coefficient and $d_{33}^{(*)}$ and $d_{13}^{(*)}$ are the longitudinal and transverse piezoelectric coefficients characterizing the dielectric response for axial and lateral compression, respectively. Unfortunately, $d_{33}^{(*)}$ and $d_{13}^{(*)}$ have opposite signs, thus resulting in a relatively small hydrostatic coupling factor $d_h^{(*)}$. For instance, PZT5A has $d_{33}^{(*)} = 374$ pC N^{-1} and $d_{13}^{(*)} = -171$ pC N^{-1}. Therefore, $d_h^{(*)} = 32$ pC N^{-1} which is small compared to $d_{33}^{(*)}$. As we will see, a polymer/piezoceramic composite can have a sensitivity that is orders of magnitude greater than a pure piezoceramic device. Using a piezo/polymer composite, the factor of 2 on the transverse piezoelectric coefficient $d_{13}^{(*)}$ in equation (1) can be lowered, or even change sign, if we use a soft matrix material or a matrix material with negative Poisson's ratio (e.g. Smith [44]), thereby ensuring a much higher hydrostatic charge coefficient.

The remainder of the paper is organized in the following way. In section 2 we describe the topology optimization procedure for two and three phases and its application to design of material structures with extremal effective behavior. The sequential linear programming method used to solve the topology optimization problem is described in section 2.2 and numerical implementation issues are discussed in section 2.3. Section 3 summarizes our work on the design of composites with extreme thermal expansion coefficients. Section 4 reviews our work on the optimal design of matrix materials for 1–3 piezocomposites. Finally, in section 5 we make concluding remarks.

2. Procedures for two- or three-phase topology optimization

We assume perfect bonding between the material phases and that the behavior of materials can be described by the linear generalized Hooke law given as

$$\begin{aligned}\sigma_{ij} &= C_{ijkl}\epsilon_{kl} - C_{ijkl}\alpha_{kl}\Delta T - C_{ijkl}d_{mkl}E_m \\ &= C_{ijkl}\epsilon_{kl} - \beta_{ij}\Delta T - e_{ijm}E_m \end{aligned} \tag{2}$$

where C_{ijkl}, σ_{ij}, ϵ_{kl}, α_{kl}, β_{ij}, d_{ijm} and e_{ijm} are the elasticity, stress, strain, thermal strain, thermal stress, piezoelectric strain and piezoelectric stress tensors, respectively, and ΔT is the temperature change and E_m is the electric field. We refer to α_{kl} as the 'thermal strain tensor' (the resulting strain of a material which is allowed to expand freely and which is subjected to increase in temperature of one unit) and to β_{ij} as the 'thermal stress tensor' (the stress in a material which is not allowed to expand and which is subjected to increase in temperature of one unit). Equivalent definitions can be made for the piezoelectric strain and stress tensors d_{ijm} and e_{ijm}. For the two- or three-phase composite of interest, the constitutive equation (2) is valid on a local scale (with superscripts (0), (1) and (2) appended to the properties, e.g. $C_{ijkl}^{(m)}$, $\alpha_{ij}^{(m)}$, $\beta_{ij}^{(m)}$, $d_{ijm}^{(m)}$ and $e_{ijm}^{(m)}$) and the macroscopic scale (with superscript (*) appended to the properties). In the latter case, the stresses and strains are averages over local stresses and strains, respectively, i.e.

$$\begin{aligned}\overline{\sigma}_{ij} &= C_{ijkl}^{(*)}\overline{\epsilon}_{kl} - C_{ijkl}^{(*)}\alpha_{kl}^{(*)}\Delta T - C_{ijkl}^{(*)}d_{mkl}^{(*)}\overline{E}_m \\ &= C_{ijkl}^{(*)}\overline{\epsilon}_{kl} - \beta_{ij}^{(*)}\Delta T - e_{ijm}^{(*)}\overline{E}_m \end{aligned} \tag{3}$$

where the overbar denotes the volume average. The effective thermoelastic and piezoelectric properties, $C_{ijkl}^{(*)}$, $\alpha_{kl}^{(*)}$, $\beta_{ij}^{(*)}$, $d_{mkl}^{(*)}$ and $e_{ijm}^{(*)}$ of the composite are computed using a numerical homogenization method as described in Sigmund and Torquato [33].

The general goal is to optimize components or combinations of components of the effective tensors by distributing, in a clever way, given amounts of one or two material phases and void within the design domain representing a base cell of a periodic material. In other words, we want to design microstructural topologies that give us some desirable overall thermoelastic properties. As will be seen later, materials with extreme thermal expansion or piezoelectric properties tend to have low overall stiffness. Thus, for practical applications, one must bound the effective stiffness or bulk moduli from below. It should also be possible to specify elastic symmetries such as orthotropy, square symmetry or isotropy of the resulting materials.

An optimization problem including these features can be written as

minimize : some effective property
variables : distribution of one or two material phases and void in the base cell
subject to : constraints on volume fractions
: orthotropy, square symmetry or isotropy constraints
: lower bound constraints on stiffness
: bounds on design variables. (4)

2.1. Formulation of the optimization problem

This subsection discusses the individual parts of the optimization problem defined in equation (4). We generally consider d-dimensional composites (with $d = 2$ or 3) that are comprised of two or three phases. In sections 3 and 4 we specialize to thermoelasticity and piezoelectricity, respectively.

2.1.1. Objective function. The objective function can be any combination of the effective coefficients given in (3). For example, suppose we wanted to minimize the isotropic thermal expansion for a two-dimensional composite, i.e. the sum of the thermal strain coefficients in the horizontal and the vertical directions. In this case, the objective function will be $f(\alpha_{ij}^{(*)}) = \alpha_{11}^{(*)} + \alpha_{22}^{(*)}$, where subscripts 11 and 22 define horizontal and vertical directions, respectively.

2.1.2. Design variables and mixture assumption. Phase 1 material has the stiffness tensor $C_{ijkl}^{(1)}$, thermal strain coefficient tensor $\alpha_{ij}^{(1)}$ and piezoelectric strain coefficient tensor $d_{ijk}^{(1)}$. Similarly, phase 2 material has the stiffness tensor $C_{ijkl}^{(2)}$, thermal strain coefficient tensor $\alpha_{ij}^{(2)}$ and piezoelectric strain coefficient tensor $d_{ijk}^{(2)}$. The stiffness tensor of the

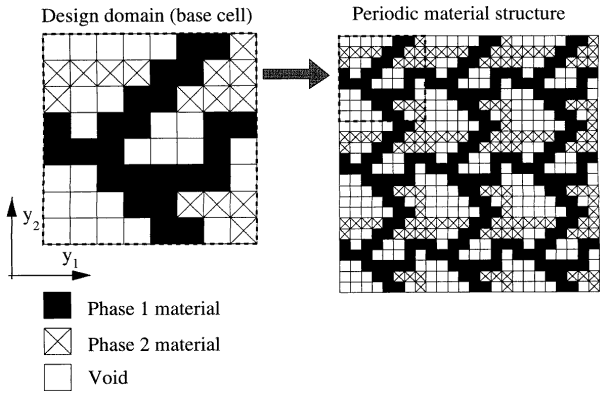

Figure 2. Design domain and discretization for a three-phase, two-dimensional topology optimization problem. Each square represents one finite element which can consist of either phase 1 or 2 material or void.

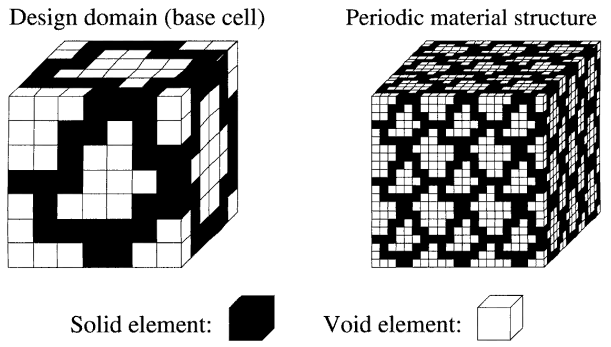

Figure 3. Design domain and discretization for a two-phase, three-dimensional topology optimization problem. Each square represents one finite element which can consist of either phase 1 material or void.

'void' phase is taken as a small number x_{min} times $C^{(1)}_{ijkl}$, respectively, where $x_{min} = 10^{-4}$, for reasons which will be explained later.

The material type, that is, material phase 1, phase 2 or void, can vary from finite element to finite element as seen in figure 2 for the three-phase, two-dimensional problem or figure 3 for the two-phase, three-dimensional problem. With a fine finite-element discretization, this allows us to define complicated composite topologies within the design domain. Having discretized the design domain (the periodic base cell) with N finite elements, the design problem consists in assigning either phase 1, 2 or void to each element such that the objective function is minimized.

Even for a small number of elements, this integer-type optimization problem becomes a huge combinatorial problem which is impossible to solve. For a small design problem with $N = 100$, the number of different distributions of the three material phases would be astronomical ($3^{100} = 5 \times 10^{47}$). As each function evaluation requires a full finite element analysis, it is hopeless to solve the optimization problem using random search methods such as genetic algorithms or simulated annealing methods, which use a large number of function evaluations and do not make use of sensitivity information. Following the idea of standard topology optimization procedures, the problem is therefore relaxed by allowing the material at a given point to be a mixture of the three phases. This makes it possible to find sensitivities with respect to design changes, which in turn allows us to use mathematical programming methods to solve the optimization problem. At the end of the optimization procedure however, we hope to have a design where each element is either void, phase 1 or phase 2 material.

Using a simple artificial mixture assumption, the local stiffness and thermal strain coefficient tensors in element e can be written as a function of the two design variables x^e_1 and x^e_2

$$C^e_{ijkl}(x^e_1, x^e_2) = (x^e_1)^\eta \left[(1 - x^e_2)C^{(1)}_{ijkl} + x^e_2 C^{(2)}_{ijkl}\right] \quad (5)$$

$$\alpha^e_{ij}(x^e_2) = (1 - x^e_2)\alpha^{(1)}_{ij} + x^e_2\alpha^{(2)}_{ij} \quad (6)$$

$$d^e_{ijk}(x^e_2) = (1 - x^e_2)d^{(1)}_{ijk} + x^e_2 d^{(2)}_{ijk} \quad (7)$$

where η is a penalization factor discussed later. The variable $x^e_1 \in [x_{min}, 1]$ can be seen as a local density variable with $x^e_1 = x_{min}$ meaning that the given element is 'void' and $x^e_1 = 1$ meaning that the given element is solid material. The variable $x^e_2 \in [0, 1]$ is a 'mixture coefficient' with $x^e_2 = 0$ meaning that the given element is pure phase 1 material and $x^e_2 = 1$ meaning that it is pure phase 2 material. The local thermal strain tensor $\alpha^e_{ij}(x^e_2)$ is not dependent on the density variable x^e_1. This can be explained by the fact that once we have chosen the local material mixture (i.e. the value of x^e_2), the thermal strain coefficient does not change with density.

It should be emphasized that the local material assumptions equations (6) only are valid for the design variables taking the extreme values. Nevertheless, during the design process we allow intermediate values meaning that we are working with artificial materials. This violation is not critical as long as we end up with a discrete design as discussed in the introduction.

Experience shows that the penalty parameter η should be given values ranging from 3 to 10 depending on the design problem. The influence of the penalty parameter can be explained as follows: Let us assume that $x^e_2 = 0$ in element e. The local stiffness tensor dependence of x^e_1 (equation (5)) can then be written as $C^e_{ijkl}(x^e_1) = (x^e_1)^\eta C^{(1)}_{(ijkl)}$. By specifying a value of η higher than one, the local stiffness for fixed $x^e_1 < 1$ is lowered, thus making it 'uneconomical' to have intermediate densities in the optimal design.

2.1.3. Constraints on volume fractions. Having defined the design variables x_1 and x_2 above, and assuming that the design domain has been discretized by N finite elements of volume Y^e, the volume fractions of the three phases can be calculated as the sums

$$c^{(1)} = \frac{1}{Y}\sum_{e=1}^{N} x^e_1(1 - x^e_2)Y^e$$

$$c^{(2)} = \frac{1}{Y}\sum_{e=1}^{N} x^e_1 x^e_2 Y^e \quad (8)$$

$$c^{(0)} = 1 - c^{(1)} - c^{(2)}$$

where Y is the volume of the base cell. For a specific design problem, we might want to constrain the volume fractions of

the phases. This can be done by defining two volume fraction constraints as

$$c^{(1)}_{min} \leqslant c^{(1)} \leqslant c^{(1)}_{max} \qquad c^{(2)}_{min} \leqslant c^{(2)} \leqslant c^{(2)}_{max} \tag{9}$$

where $c^{(1)}_{min}$, $c^{(2)}_{min}$, $c^{(1)}_{max}$ and $c^{(2)}_{max}$ are lower and upper bounds on the volume fractions of material 1 and 2, respectively. By setting the lower bound constraint equal to the upper bound constraint, it is possible to fix the volume fractions of the individual phases.

2.1.4. Isotropy or square symmetry constraints. For the purpose of designing materials with either orthotropic, square symmetric or isotropic elastic parameters, such constraints must be implemented in the optimization problem. Orthotropy of the materials can be obtained simply by specifying at least one geometrical symmetry axis in the base cell.

To illustrate this point, we consider for simplicity orthotropy in two dimensions with the understanding that similar statements can be made for three-dimensional composites. Assuming that a material structure is orthotropic, the condition for square symmetry of the elasticity tensor is that $C^{(*)}_{1111} - C^{(*)}_{2222} = 0$, and the conditions for isotropy of the elasticity tensor under the plane stress assumption are that $C^{(*)}_{1111} - C^{(*)}_{2222} = 0$ and $(C^{(*)}_{1111} + C^{(*)}_{2222}) - 2(C^{(*)}_{1122} + 2C^{(*)}_{1212}) = 0$. Such conditions are difficult to implement as equality constraints in an optimization problem because the starting guess might be infeasible (i.e. anisotropic). Therefore, it is chosen to implement the constraints as a penalty function added to the cost function. The penalty function is defined as the squared error in obtaining either square symmetry, elastic or thermal isotropy, times the penalization factors r_1, r_2 and r_3, respectively. It should be noted here that three 60 degree symmetry lines of a microstructure is a sufficient but not a necessary condition for isotropy. Indeed, this paper shows examples of isotropic material structures with only one line of symmetry. The errors in obtaining square symmetry or isotropy, respectively, can be written as

$$\text{error}_{sq} = \frac{(C^{(*)}_{1111} - C^{(*)}_{2222})^2}{(C^{(*)}_{1111} + C^{(*)}_{2222})^2}$$

$$\text{error}_{iso} = \frac{\left[(C^{(*)}_{1111} + C^{(*)}_{2222}) - 2(C^{(*)}_{1122} + 2C^{(*)}_{1212})\right]^2}{(C^{(*)}_{1111} + C^{(*)}_{2222})^2} + \text{error}_{sq}. \tag{10}$$

Expressions similar to error_{sq} and error_{iso} are also known in the literature of composite materials (e.g. [45]) as the practical composite parameters U_2 and U_3. The error for thermal isotropy is denoted by error_{therm}.

2.1.5. Lower bound constraints on effective stiffness. Low stiffness is generally undesirable and therefore we will generally introduce a lower bound constraint on the Young's moduli $E^{(*)}_i$ in the ith direction or on the bulk modulus $k^{(*)}$ of the material. Such constraints can be written as $g_{i(min)} \leqslant g_i(C^{(*)}_{ijkl})$. For example, in the case of 2D isotropic materials, we can impose a lower bound constraint on the bulk modulus ($k^{(*)}_{min} \leqslant k^{(*)} = ((C^{(*)}_{1111} + C^{(*)}_{2222})/2 + C^{(*)}_{1122})/2$).

2.1.6. Lower bound constraints on design variables. For computational reasons (singularity of the stiffness matrix in the finite element formulation), the lower bound on design variable x^e_1 is set to x_{min}, not zero ($x_{min} = 10^{-4}$). Numerical experiments show that the 'void' regions have practically no structural significance and can be regarded as real void regions. The bounds on the design variables can thus be written as $0 < x_{min} \leqslant x^e_1 \leqslant 1$ and $0 \leqslant x^e_2 \leqslant 1$.

2.1.7. The final optimization problem. An optimization problem including the above mentioned features can now be written as

$$\begin{aligned}
\text{minimize} &: \Phi(\boldsymbol{x}_1,\ \boldsymbol{x}_2) = f(\alpha^{(*)}_{ij},\ \beta^{(*)}_{ij}) + r_1\,\text{error}_{sqr} \\
&\quad + r_2\,\text{error}_{iso} + r_3\,\text{error}_{therm} \\
\text{subject to} &: g_{i(min)} \leqslant g_i(C^{(*)}_{ijkl}) \qquad i = 1, \ldots, M \\
&: c^{(1)}_{min} \leqslant c^{(1)} \leqslant c^{(1)}_{max} \\
&: c^{(2)}_{min} \leqslant c^{(2)} \leqslant c^{(2)}_{max} \\
&: \mathbf{0} < \boldsymbol{x}_{min} \leqslant \boldsymbol{x}_1 \leqslant \mathbf{1} \\
&: \mathbf{0} \leqslant \boldsymbol{x}_2 \leqslant \mathbf{1}
\end{aligned} \tag{11}$$

where $\boldsymbol{x}_1$ and $\boldsymbol{x}_2$ are the N-vectors containing the design variables, the three penalty parameters r_i can be set to zero or non-zero values, depending on the desired symmetry type, and M is the number of constraints.

2.2. Sequential linear programming method

Topology optimization problems in the literature often consist in the optimization of a simple energy functional (e.g. compliance or eigenfrequencies) with a single constraint on material resource, and these problems can therefore be solved very efficiently using optimality criterion methods. In this paper, however, we are considering several different objective functions and multiple constraints which can not be written in energy forms and therefore it will be cumbersome if not impossible to formulate the optimization problem as an optimality criterion problem. Instead we will use a mathematical programming method called sequential linear programming (SLP), which consists in the sequential solving of an approximate linear subproblem, obtained by writing linear Taylor series expansions for the objective and constraint functions. The SLP method was successfully used in optimization of truss structures [46] and was evaluated as a robust, efficient and easy to use optimization algorithm in a review paper [47].

Using the sequential linear programming method, the optimization problem equation (11) is solved iteratively. In each iteration step, the optimization problem is linearized around the current design point $\{\boldsymbol{x}_1, \boldsymbol{x}_2\}$ using the first part of a Taylor series expansion and the vector of optimal design changes $\{\Delta\boldsymbol{x}_1, \Delta\boldsymbol{x}_2\}$ is found by solving the linear programming problem

$$\begin{aligned}
\text{minimize} &: \Phi + \left\{\frac{\partial\Phi}{\partial\boldsymbol{x}_1}, \frac{\partial\Phi}{\partial\boldsymbol{x}_2}\right\}^T \{\Delta\boldsymbol{x}_1, \Delta\boldsymbol{x}_2\} \\
\text{subject to} &: g_{i(min)} - g_i \leqslant \left\{\frac{\partial g}{\partial\boldsymbol{x}_1}, \frac{\partial g}{\partial\boldsymbol{x}_2}\right\}^T \{\Delta\boldsymbol{x}_1, \Delta\boldsymbol{x}_2\} \\
&\quad i = 1, \ldots, M
\end{aligned}$$

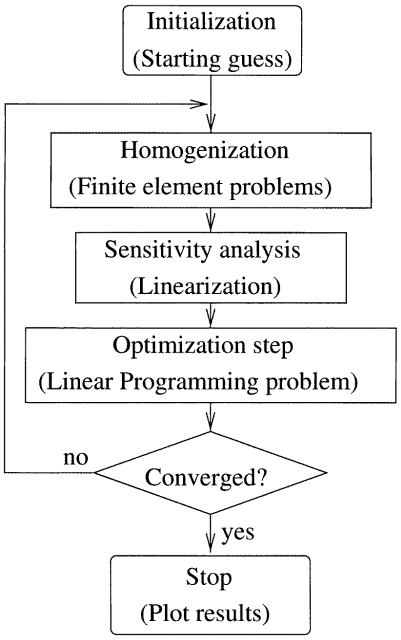

Figure 4. Flowchart of the design algorithm.

$$
\begin{aligned}
&: c_{min}^{(1)} - c^{(1)} \leqslant \left\{ \frac{\partial c^{(1)}}{\partial \boldsymbol{x}_1}, \frac{\partial c^{(1)}}{\partial \boldsymbol{x}_2} \right\}^T \{\Delta \boldsymbol{x}_1, \Delta \boldsymbol{x}_2\} \\
&\quad \leqslant c_{max}^{(1)} - c^{(1)} \\
&: c_{2min} - c^{(2)} \leqslant \left\{ \frac{\partial c^{(2)}}{\partial \boldsymbol{x}_1}, \frac{\partial c^{(2)}}{\partial \boldsymbol{x}_2} \right\}^T \{\Delta \boldsymbol{x}_1, \Delta \boldsymbol{x}_2\} \\
&\quad \leqslant c_{2max} - c^{(2)} \\
&: \{\Delta \boldsymbol{x}_{1L}, \Delta \boldsymbol{x}_{2L}\} \leqslant \{\Delta \boldsymbol{x}_1, \Delta \boldsymbol{x}_2\} \leqslant \{\Delta \boldsymbol{x}_{1U}, \Delta \boldsymbol{x}_{2U}\}
\end{aligned} \tag{12}
$$

where $\Delta \boldsymbol{x}_{1L}$, $\Delta \boldsymbol{x}_{2L}$, $\Delta \boldsymbol{x}_{1U}$ and $\Delta \boldsymbol{x}_{2U}$ are move-limits on the design variables. The move-limits are adjusted for the absolute limits given in equations (11).

The applied move-limit strategy is important for the stable convergence of the algorithm. Here we use the simple rule that the move-limit for a specific design variable is increased by a factor of 1.4 if the change in the design variable has the same sign for two subsequent steps. Similarly the move-limit is decreased by a factor of 0.6 if the change in the design variable has opposite signs for two subsequent steps.

2.3. Numerical implementation issues

This subsection describes the numerical implementation of the three-phase topology optimization problem including the finite-element discretization and procedures, the linear programming package DSPLP [48] from the SLATEC library, control of move-limits and a flowchart of the procedure.

A flowchart of the design algorithm is shown in figure 4. The individual steps of the design procedure are described in the following.

2.3.1. Initialization. First, we initialize the design problem by selecting the objective function, specifying a lower bound on the stiffness, selecting isotropy type and symmetry lines. For the 2D case, we choose the design domain discretization, using 900 or 3600 four-node linear displacement finite elements, corresponding to 30 by 30 or 60 by 60 element discretizations, depending on accuracy demands and available computing time. To save computer time, a design problem can first be solved on a 30 by 30 element mesh. When a solution has been reached, each of the elements is divided into four and the procedure is continued until convergence. For the 3D case, we use 16 by 16 by 16 (= 4096), 8-node trilinear elements.

2.3.2. Starting guess. The starting distribution of densities and material types (i.e. starting values of the design variable vectors $\boldsymbol{x}_1$ and $\boldsymbol{x}_2$) is up to the user. Having absolutely no idea of what the solution will look like, a random distribution of densities and material types is chosen as the starting guess. If the user has an idea of what the solution will look like or he has an old solution to a similar problem, a considerable amount of computing time is saved by using this (old) topology as a starting guess.

2.3.3. Homogenization step. The equilibrium equations for the homogenization problem derived in Sigmund and Torquato [33] are solved using the finite-element method applied to calculation of effective material properties in [36, 37].

2.3.4. Sensitivity analysis. The sensitivity analysis necessary to solve the linear programming problem in equation (12) is derived in Sigmund and Torquato [33]. The computation of the sensitivities is fast because they can be found from the strain fields already computed by the homogenization procedure.

2.3.5. Linear programming problem. The linear programming problem eqution (12) is solved using a linear programming solver DSPLP [48] from the SLATEC library. As the optimization is non-sparse, the DSPLP routine is invoked with an option for no sparsity. Nevertheless, the routine has proven faster and demands less storage space than other LP-algorithm tests. Recent investigations have shown that other mathematical programming methods may be more efficient in solving topology optimization problems (e.g. [14]).

2.3.6. Convergence. The iterative design procedure is repeated until the change in each design variable from step to step is lower than 10^{-4} (by experience).

2.3.7. Problems related to topology optimization. Applying the topology optimization method to different design problems, one often encounters regions of alternating solid and void elements, referred to as checkerboards, in the 'optimal solutions'. These regions appear due to bad numerical modeling and must be avoided. Furthermore, there is a strong mesh-dependency meaning that topologically different solutions appear when the mesh is changed or refined. The mesh-dependency is due to non-existence or

non-uniqueness of solutions. For further explanations of the checkerboard and mesh-dependency problems, the reader is referred to a recent review paper [49]. To avoid the checkerboard and mesh-dependency problems we here use the 'mesh-independency scheme' suggested in [18, 19] (see also [49]).

2.3.8. Local minima. The topology optimization problem is very prone to converge to local minima. However, introducing the mesh-independency scheme [18, 19] makes it possible to prevent this problem to a certain extent. Solving a cell design problem is typically done as follows. First we solve the optimization problem with a low value of the low-pass filter parameter, i.e., we do not allow rapid variation in the element densities. This results in a design with large areas of intermediate densities but it also prevents the design converging to a local minimum (binary design). Gradually, we increase the low-pass filter parameter, in turn letting the design problem converge. In that way, we gradually arrive at a solution which is entirely binary and which is, hopefully, a global optimum. To make sure that the actually obtained microstructures are indeed global optima, the same optimization problem is always solved using differing starting guesses, move-limit strategies and choices of low-pass filter parameter and penalty parameter η. However, topologically different solutions with similar values of the objective function have been found when solving specific design problems. Solutions which are 'shifted' (translated half a base cell dimension) of other solutions have also been encountered. The fact that the effective properties of the design examples are close to theoretical bounds supports our belief that we are finding the optimal topologies with the proposed design procedure.

2.3.9. Computing time. For the 2D problems, one design iteration typically takes three seconds (30 by 30 element discretization) or 20 seconds (60 by 60 element discretization) on an Indigo 2 work station. To arrive at an optimal solution, depending on starting guess, a couple of thousand iterations may be needed. For 3D problems each iteration may take 2 minutes (for a 16 by 16 by 16 element discretization).

3. Thermoelastic properties

In this section, we review in some detail our work on the use of topology optimization to design three-phase, two-dimensional composites with extremal thermal expansion behavior [33, 34].

3.1. Rigorous bounds

Rigorous bounds on the effective coefficients of three-phase, *isotropic* composites serve to benchmark the design algorithm. Here, for simplicity, we assume that the constituent phases are isotropic which implies that they can be described by their Young's moduli $E^{(0)}$, $E^{(1)}$ and $E^{(2)}$, their Poisson's ratios $\nu^{(0)}$, $\nu^{(1)}$ and $\nu^{(2)}$ and their thermal strain coefficients $\alpha^{(0)}$, $\alpha^{(1)}$ and $\alpha^{(2)}$. It is also assumed that

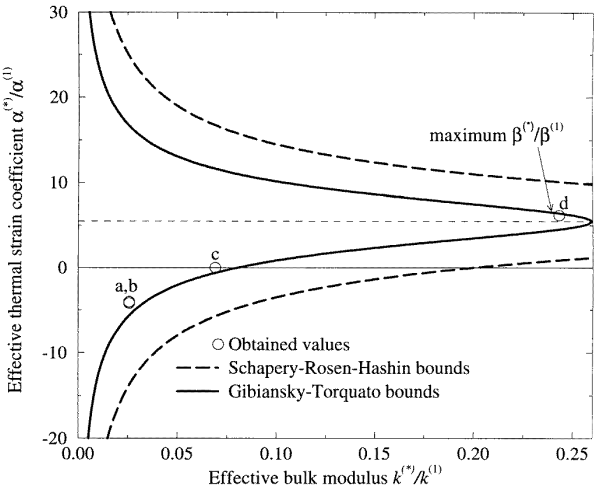

Figure 5. Bounds for three-phase design example. The circles with letters a–d denote the computed values for the microstructures of the four design examples.

the composite is macroscopicically isotropic. The bulk and shear moduli of the phases are then

$$k^{(i)} = \frac{E^{(i)}}{2(1-\nu^{(i)})} \qquad \mu^{(i)} = \frac{E^{(i)}}{2(1+\nu^{(i)})} \qquad i = 0, 1, 2. \tag{13}$$

Bounds on the effective thermal strain coefficient $\alpha^{(L)} \leqslant \alpha^{(*)} \leqslant \alpha^{(U)}$ of three-phase, isotropic composites were found in [50, 51]. A bounded domain of possible effective bulk moduli and thermal strain coefficients for a specific choice of constituent phases is shown in figure 5. We found that the proposed design method did not yield pairs $(k^{(*)},\alpha^{(*)})$ that were close to the 26-year-old Schapery–Rosen–Hashin bounds [51]. There were two possible explanations for this discrepancy: either the design method could not find the optimal solutions, or the bounds themselves could be improved upon. Indeed, the latter explanation turned out to be true. Inspired by the above mentioned discrepancy Gibiansky and Torquato [52] recently found improved bounds, which are also shown in figure 5. As will be seen in the subsequent section, the solutions obtained by the design procedure are very close to the new bounds.

Examination of the thermoelastic bounds in figure 5 reveals that extreme values (e.g. negative values) of thermal strain coefficients only are possible for low bulk moduli. If we simply tried to minimize/maximize the thermal strain $\alpha^{(*)}$, we would end up with a very weak material. Therefore, there is a tradeoff between extremizing thermal strain coefficients on the one hand and ending up with a stiff material on the other.

3.2. Design examples

In this section, we will first discuss design examples with mixtures of hypothetical materials. These examples are used to benchmark the design algorithm for three-phase design. We will also study other design examples that utilize real materials as constituent phases.

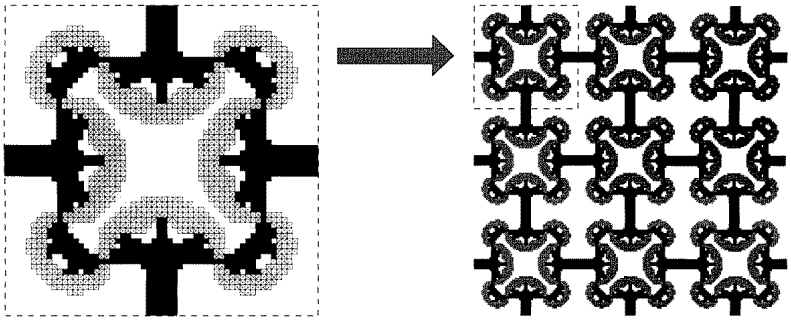

Figure 6. Design example (b): optimal microstructures for minimization of effective thermal strain coefficient corresponding to the circle b in figure 5. The white regions denote void (phase 0), the filled regions consist of low-expansion material (phase 1) and the cross-hatched regions consist of high-expansion material (phase 2).

3.2.1. Plotting results. During the iterative procedure, a Postscript plot of the topology is generated every ten iterations. The plot shows the current density and material distribution in the base cell, thus allowing the user to follow the evolution of the microstructure and interact if necessary. The plots in the following sections show the optimal density and material type distributions for the different design problems. If an element is predominantly material phase two (i.e., $x_2^e > 0.5$), the element is illustrated by a cross with grey scale denoting the density x_1^e; white means void ($x_1^e = x_{min}$) and black means solid ($x_1^e = 1$). If the element is predominantly material phase one (i.e., $x_2^e < 0.5$), it is shown as a filled rectangle with grey values interpreted as before. For all examples, we both show the resulting topologies represented by a single base cell (the design domain) and as a repeated microstructure consisting of 3 by 3 base cells.

3.3. Hypothetical designs

The Gibiansky–Torquato three-phase bounds are used to benchmark the design algorithm for three-phase design. The material data for the two phases are chosen as $E^{(1)}/E^{(2)} = 1$, $\nu^{(1)} = \nu^{(2)} = 0.3$, $\alpha^{(2)}/\alpha^{(1)} = 10$, and the volume fractions are prescribed to be $c^{(1)} = c^{(2)} = 0.25$ (i.e. $c^{(0)} = 0.5$). *Note that the volume fractions c_i are held fixed for this hypothetical composite, to allow for comparison with the bounds and for easy interpretation of the results.*

Four three-phase design examples, constrained to be elastically isotropic, are considered as follows:

(a) Minimization of the *isotropic* thermal strain coefficient $\alpha^{(*)}/\alpha^{(1)}$ with a lower bound constraint on the effective bulk modulus given as 10% of the theoretically attainable bulk modulus, i.e. $k^{(*)}/k^{(1)} = 0.0258$. Horizontal geometric symmetry is specified.
(b) Same as design example (a) but with horizontal, vertical and diagonal (geometric) symmetry.
(c) Maximization of bulk modulus $k^{(*)}/k^{(1)}$ for fixed zero thermal expansion $\alpha^{(*)}/\alpha^{(1)} = 0$. Horizontal geometric symmetry is specified.
(d) Maximization of isotropic thermal stress coefficient $\beta^{(*)}/\beta^{(1)}$ with horizontal, vertical and diagonal geometric symmetry.

The Schapery–Rosen–Hashin and Gibiansky–Torquato theoretical bounds are shown figure 5. In examples (a) and (b), the lower bound on the possible thermal strain coefficient is $-5.567 \leqslant \alpha^{(*)}/\alpha^{(1)}$. In example (c), the upper bound on possible bulk modulus for zero thermal expansion is $k^{(*)}/k^{(1)} \leqslant 0.0692$. The upper bound on the thermal stress coefficient in design example (d) is $\beta^{(*)}/\beta^{(1)} \leqslant 3.15$ (for $k^{(*)}/k^{(1)} = 0.237$).

The effective properties for examples (a)–(d) are shown in table 1 and plotted as small circles in figure 5. Studying the graph in figure 5, we see that the obtained effective values are far away from the original Schapery–Rosen–Hashin bounds. This discrepancy inspired Gibiansky and Torquato to try to improve the bounds and indeed improvement was possible as seen in figure 5. The effective values of the examples (a)–(d) are still somewhat away from the improved bounds. This can be explained by the fact that the new bounds by Gibiansky and Torquato have not been proven to be optimal. Furthermore, it is our experience that a finer finite-element mesh makes it possible to get closer to the bounds. In example (a), the minimum thermal strain coefficient obtained for a 30 by 30 mesh is $\alpha^{(*)} = -3.59$ and $\alpha^{(*)} = -4.17$ for the 60 by 60 element discretization shown in figure 6. Due to computer time limitations, it has not been possible to try out finer discretizations.

The resulting topology for design example (b) is shown in figures 6. The actual mechanisms behind the extreme thermal expansion coefficients of the material structures can be difficult to understand. To visualize one of the mechanisms, the (exaggerated) displacement, due to an increase in temperature of the microstructure in figure 6 (bottom), is shown in figure 7. Studying figure 7, we note that there appears to be contact between parts of the microstructure. This contact is only due to the magnification of the displacements used in the illustration. The simple linear modeling used here can not take such problems into account. Nevertheless, it would be interesting to extend the analysis to include non-linear behavior including contact, which would open up a whole new world of interesting design possibilities. We will leave these extensions to future studies.

When allowing low bulk moduli (as in example (b)), the main mechanism behind the extreme (negative) thermal expansion is the *reentrant cell structure* having bimaterial components which bend and cause large deformation when heated. The bimaterial interfaces of design example (b) bend and make the cell contract, similar to the behavior of negative Poisson's ratio materials [53]. The topological results for

Table 1. Thermoelastic parameters for optimal three-phase microstructures composed of hypothetical materials compared with the bounds.

Example	Objective constraint	$k^{(*)}/k^{(1)}$ (bound)	$\nu^{(*)}$	$\alpha^{(*)}/\alpha^{(1)}$ (bound)	$\beta^{(*)}/\beta^{(1)}$ (bound)
(a)	Min. $\alpha^{(*)}/\alpha^{(1)}$ $k^{(*)}/k^{(1)} \geqslant 0.0258$	0.0258	0.039	−4.17 (−5.567)	
(b)	Min. $\alpha^{(*)}/\alpha^{(1)}$ $k^{(*)}/k^{(1)} \geqslant 0.0258$	0.0258	0.51	−4.02 (−5.567)	
(c)	Max. $k^{(*)}/k^{(1)}$ $\alpha^{(*)}/\alpha^{(1)} \leqslant 0.0$	0.692 (0.0814)	0.54	0	
(d)	Max. $\beta^{(*)}/\beta^{(1)}$	0.243	0.51		3.01 (3.15)

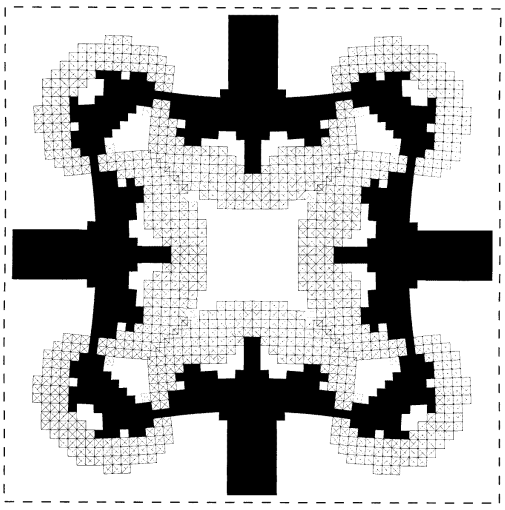

Figure 7. Thermal displacement of the negative thermal expansion microstructure in figure 6 (bottom).

the designs (a), (c) and (d) are quite different from (b). The interested reader is referred to works of Sigmund and Torquato [33, 34] to see these differences.

3.4. Mixtures of real materials

For the design of new materials with extreme thermal expansion coefficients, the two base materials should be of equal stiffness but widely differing thermal strain coefficients. Two materials fulfilling this requirement are isotropic Invar (Fe–36% Ni) and nickel as discussed in the introduction. *For the next design examples, the volume fractions of the material phases are unconstrained.* This will allow for a wider range of minimum and maximum values, in contrast to the hypothetical examples (a)–(d) in which the volume fractions were fixed.

The material properties of Invar and nickel can be found in [54]. The Young's moduli are 150 GPa and 200 GPa, respectively, Poisson's ratios are 0.31 for both and the thermal expansion coefficients are 0.8 μm mK^{-1} and 13.4 μm mK^{-1}, respectively.

(e) Minimization of the *isotropic* thermal stress coefficient $\beta^{(*)}$. Horizontal geometric symmetry is specified.
(f) Minimization of the *vertical* thermal stress coefficient $\beta_{22}^{(*)}$. Horizontal and vertical symmetry is specified.
(g) Minimization of the *vertical* thermal stress $E_2^{(*)}\alpha_{22}^{(*)}$. Horizontal and vertical symmetry is specified.
(h) Maximization of the *vertical* strain $(\alpha^*)_{22}$ with constraint on vertical Young's modulus $E_2^{(*)} \geqslant 5$ GPa. Horizontal and vertical symmetry is specified.

The resulting topologies are shown in figures 8, 9 and 10, and their effective properties are shown in table 2.

To overcome the positive thermal expansion of other surrounding materials, we seek to maximize the *contraction force*, i.e., minimize the isotropic thermal stress coefficient as in example (e). The obtained *isotropic* contraction stress of example (e) is $\beta^{(*)} = -77.6$ GPa. By relaxing the isotropy requirement and allowing orthotropic materials the *directional* contraction stress can be increased. In example (f) we minimize the value of $\beta_{22}^{(*)}$ and obtain the effective value $\beta_{22}^{(*)} = -210$ GPa. Minimizing the value of $\beta_{22}^{(*)}$ gives us a composite which for *fixed boundaries* has high contraction force (remember that the thermal stress coefficient $\beta^{(*)}$ is the stress in a material constrained at the boundaries). If we want to maximize the contraction force for a material with free boundaries, we should minimize the product $(E_2^*)(\alpha^*)_{22}$ as done in example (h). The 'free boundary' stress of example (f) is $(E_2^*)(\alpha^*)_{22} = -14$ GPa, whereas the 'free boundary' stress of example (g) is $(E_2^*)(\alpha^*)_{22} = -138$ GPa.

If we want to *maximize* the expansion stress of the composite, the best choice would be to take solid nickel material both for the isotropic and the directional cases.

The isotropic negative thermal expansion materials in examples (a), (b) and (e) all have positive Poisson's ratios (0.04, 0.52 and 0.055, respectively), *showing that there is no mechanistic relationship between negative thermal expansion and negative Poisson's ratio*.

In example (h) we see again that allowing orthotropy can lead to high *directional* expansion coefficients. The vertical coefficient $(\alpha^*)_{22}$ of example (h) is 2.6 times higher than for solid nickel, but at the cost of a low vertical Young's modulus (2.5% of solid nickel).

4. Piezocomposite design

In this section, we review our work on the use of topology optimization to design three-dimensional, anisotropic porous composites with negative Poisson's ratios (in certain directions) for use as the matrix phase in 1–3 piezocomposites [21]. A schematic of the piezocomposite is shown in figure 1. Thus, we seek the optimal design of the matrix shown in this figure.

The use of piezocomposites in hydrophone design has been studied in several papers. Hydrophones composed

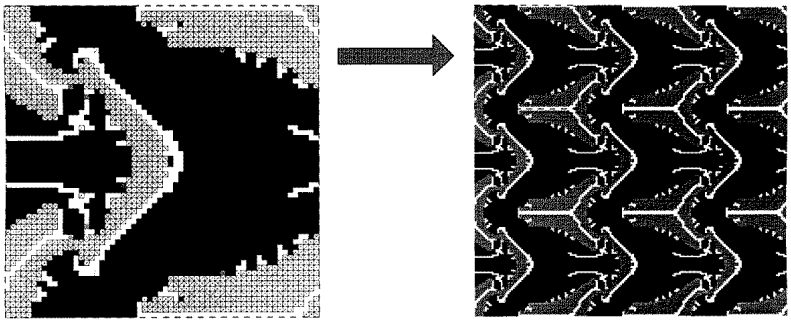

Figure 8. Example (e): optimal microstructure for minimization of the isotropic thermal stress coefficient $\beta^{(*)}$. The white regions denote void (phase 0), the filled regions consist of Invar (phase 1) and the cross-hatched regions consist of nickel (phase 2).

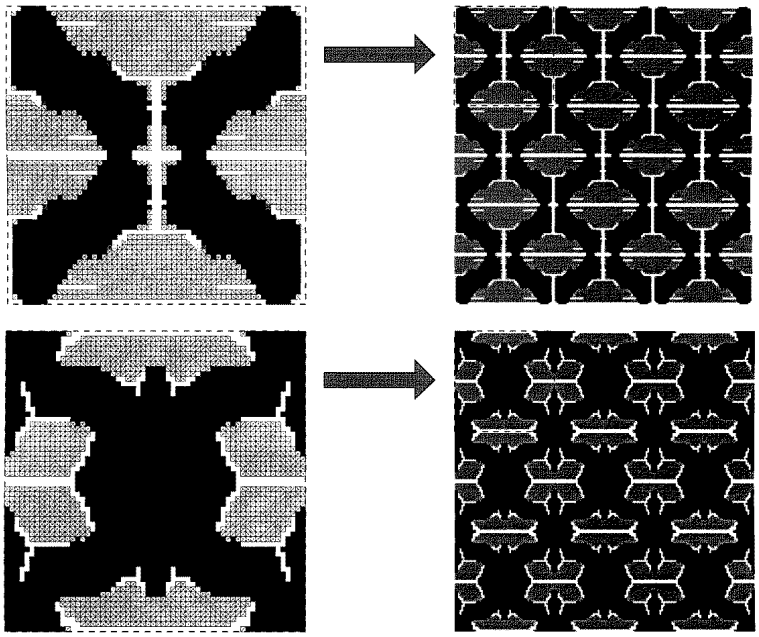

Figure 9. Examples (f) (top) and (g) (bottom): optimal microstructures for minimization of thermal stress coefficient $\beta_{22}^{(*)}$ (top) and minimization of vertical contraction stress $E_2^{(*)}\alpha_{22}^{(*)}$. The white regions denote void (phase 0), the filled regions consist of Invar (phase 1) and the cross-hatched regions consist of nickel (phase 2).

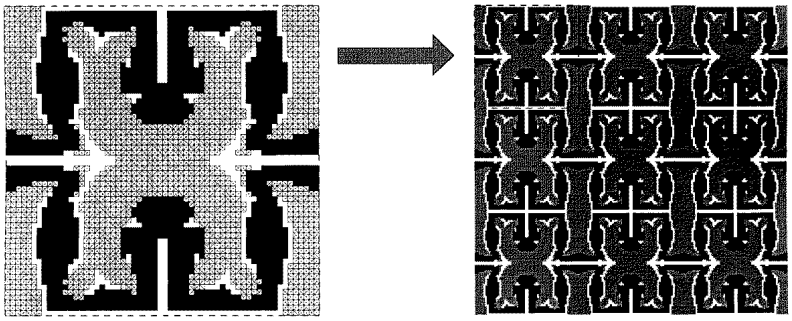

Figure 10. Example (h): optimal microstructure for maximization of thermal strain in the vertical direction $\alpha_{22}^{(*)}$. The white regions denote void (phase 0), the filled regions consist of Invar (phase 1) and the cross-hatched regions consist of nickel (phase 2).

of piezoelectric rods in solid polymer matrices have been tested experimentally in [55, 43, 56]. Using simple models in which the elastic and electric fields were taken to be uniform in the different phases, Haun and Newnham [57], Chan and Unsworth [58] and Smith [44] qualitatively explained the enhancement due to the Poisson ratio effect. A more sophisticated analysis has recently been given by Avellaneda and Swart [59] using the so-called *differential-effective-medium approximation*. They found the effective performance factors: the hydrostatic charge coefficient d_h^*, the hydrostatic voltage coefficient g_h^* and

Table 2. Thermoelastic parameters for optimal microstructures made of Invar (phase 1) and nickel (phase 2).

Example	Objective	$\alpha^{(*)}$ ($\alpha_{11}^{(*)}/\alpha_{22}^{(*)}$) ($\mu$m mK^{-1})	$E^{(*)}$ ($E_1^{(*)}/E_2^{(*)}$) (GPa)	$\nu^{(*)}$ ($\nu_{12}^{(*)}/\nu_{21}^{(*)}$)	$\beta^{(*)}$ ($\beta_{11}^{(*)}/\beta_{22}^{(*)}$) (kPa K^{-1})	$c^{(1)}/c^{(2)}$
Invar		0.8	150	0.31	174	1/0
Nickel	(Max. $\beta^{(*)}$)	13.4	200	0.31	3884	0/1
(e) Figure 8	Min. $\beta^{(*)}$	–4.97	14.8	0.055	−77.6	0.60/0.28
(f) Figure 9	Min. $\beta_{22}^{(*)}$	9.98/−1.59	9.19/8.75	−0.80/−0.76	258/−210	0.49/0.38
(g) Figure 9	Min. $E_2^{(*)}\alpha_{22}^{(*)}$	5.42/−4.68	69.9/29.5	0.059/0.025	372/−129	0.60/0.30
(h) Figure 10	Max. $\alpha_{22}^{(*)}$	23.4/35.0	1.09/5.00	−0.14/−0.62	2.01/174	0.38/0.46

the electromechanical coupling factor k_h^* as functions of the effective moduli of the composite and simple structural parameters. In [59], it is assumed that the matrix material is isotropic.

Recently, Gibiansky and Torquato [60] found theoretical bounds for hydrophone design using the elastic properties of the matrix material as design variables. In contrast to Avellaneda and Swart [59], they allowed the matrix material to be transversely isotropic. However, they did not consider finding the actual matrix microstructure corresponding to the optimal elastic properties. In very recent work [21], we took the first steps towards closing this gap by designing the optimal microstructural matrix topology simultaneously with the optimization of the hydrophone performance.

Less research has been devoted to the design of three-dimensional microstructures. Three-dimensional optimal rigidity materials can be made as microstructures with several length scales and the design of trusslike microstructures with extreme elastic properties as described in Sigmund [31]. However, neither of these methods give practically realizable microstructures.

Sigmund *et al* [21] have designed practically realizable three-dimensional microstructures using the topology optimization method. They did so in the context of finding matrices that optimize the performance characteristics of 1–3 piezocomposites. They considered fixed topology of the rods (vertical rods) and assumed them to be PZT. The microstructural topology of the matrix material and the volume fraction of piezoelectric rods were taken to be the design variables. Using the topology optimization method, they found the optimal matrix topology using the analytical formulas for the effective piezoelectric moduli developed by Avellaneda and Swart [59]. In contrast to this two-step procedure, Silva *et al* [35] have used a direct optimization approach for the case of two-dimensional piezocomposites, but with a fixed rod topology as we assumed.

4.1. Design examples

Sigmund *et al* [21] considered designing optimal matrices (using a specific polymer material) for four different piezocomposites. Here we discuss only two of these designs: piezocomposites with maximum $d_h^{(*)}$ and maximum $(k_h^{(*)})^2$. The base cell is discretized with 16 by 16 by 16 (= 4096) cubic finite elements. By variable linking due to symmetry, the number of design variables (element densities) can be decreased to $4096/8 = 512$.

4.1.1. Properties of the piezoceramic and polymer. The ceramic rods and the polymer (that will make up the solid material in the designed porous matrix) are specified. The actual properties of the PZT-ceramic rods are taken as

$$\begin{aligned} C^{(i)} &= \begin{bmatrix} 120 & 75 & 75 \\ 75 & 120 & 75 \\ 75 & 75 & 111 \end{bmatrix} \times 10^9 \text{ Pa} \\ e_{13}^{(i)} &= -5.4 \text{ C m}^{-2} \\ e_{33}^{(i)} &= 15.8 \text{ C m}^{-2} \\ \varepsilon_{33}^{T(i)} &= 827\varepsilon_0 \end{aligned} \tag{14}$$

where $\varepsilon_{33}^{T(i)}$ is the free body axial dielectric constant. The Young's modulus and the Poisson's ratio of the amorphous polymer are taken to be 2.5×10^9 Pa and 0.37, respectively. Therefore, the polymer stiffness tensor is given by

$$\begin{aligned} C^{(p)} &= \begin{bmatrix} 4.4 & 2.6 & 2.6 \\ 2.6 & 4.4 & 2.6 \\ 2.6 & 2.6 & 4.4 \end{bmatrix} \times 10^9 \text{ Pa} \\ e_{13}^{(p)} &= e_{33}^{(p)} = 0 \\ \varepsilon_{33}^{T(p)} &= 3.5\varepsilon_0. \end{aligned} \tag{15}$$

The value of the dielectric constant in vacuum is

$$\varepsilon_0 = \frac{1}{4\pi} \frac{10^{-9}}{8.987\,55} \frac{\text{C}^2}{\text{N m}^2}. \tag{16}$$

The minimum value of the in-plane bulk modulus of the matrix material is chosen as 3% of solid polymer i.e. $K_{min} = 0.11 \times 10^9$ Pa and the minimum volume fraction of the piezoceramic is $f_{min} = 0.01$.

4.1.2. Optimization. Our objective is to design the best matrix material (consisting of voids distributed throughout polymer) in order to maximize hydrophone performance indices. The effective hydrostatic charge coefficient $d_h^{(*)}$ is defined as

$$d_h^{(*)}(f, \boldsymbol{x}) = d_{33}^{(*)}(f, \boldsymbol{x}) + 2d_{13}^{(*)}(f, \boldsymbol{x}) \tag{17}$$

where we explicitly include the dependence on the element densities $\boldsymbol{x}$ of the discretized base cell (modeling the matrix material) and the volume fraction of piezoelectric rods f embedded in the matrix. The effective non-dimensional electromechanical coupling factor

$$\left(k_h^{(*)}\right)^2(f, \boldsymbol{x}) = \frac{(d_h^{(*)}(f, \boldsymbol{x}))^2}{\varepsilon_{33}^{T(*)}(f, \boldsymbol{x}) s_h^{(*)}(f, \boldsymbol{x})} \tag{18}$$

Table 3. Effective values for pure piezoceramic, optimal piezocomposite with solid matrix and optimal piezocomposite with topology-designed matrix.

Ex.	Objective	f	$d_{13}^{(*)}$ (pC N^{-1})	$d_{33}^{(*)}$ (pC N^{-1})	$d_h^{(*)}$ (pC N^{-1})	$d_h^{(*)} g_h^{(*)}$ p (Pa)$^{-1}$	$(k_h^{(*)})^2$	$s_h^{(*)}$ n (Pa)$^{-1}$
Pure ceramic								
		1.0	−171	374	32	0.068	0.0061	0.011
Solid matrix with rods								
	Max. $d_h^{(*)}$	0.211	−125	318	68	1.50	0.0065	0.22
	Max. $(k_h^{(*)})^2$	0.041	–67	167	41	3.87	0.0135	0.29
Optimal matrix with rods								
a	Max. $d_h^{(*)}$	0.042	75	346	497	399	0.049	7.9
b	Max. $(k_h^{(*)})^2$	0.010	–4	356	348	685	0.292	2.3

where $\varepsilon_{33}^{T(*)}(f, \boldsymbol{x})$ is the effective free body axial dielectric constant and $s_h^{(*)}(f, \boldsymbol{x})$ is the effective dilatational compliance. We choose to work with the squared electromechanical coupling factor since this has a physical meaning of electrical energy output divided by mechanical energy input.

Using the analysis of Avellaneda and Swart [59], we can re-express all of the above effective relations explicitly in terms of the effective transverse bulk modulus of the composite [21]. Following Gibiansky and Torquato [52], the effective transverse bulk modulus is taken to be equal to the lower Hashin–Shtrikman bound, implying that the piezoelectric rods should be ordered in a hexagonal array to ensure optimality of the composite. Thus, first we compute the effective properties of the matrix composite material (polymer and voids) and then we calculate the effective performance indices of the piezocomposite (composed of the piezoceramic rods and matrix composite material) via the aforementioned analytical expressions.

Given the piezoelectric performance coefficients in terms of the matrix microstructural design variables $\boldsymbol{x}$ (the element densities) and the volume fraction of the piezoelectric rods f, we consider two design examples:

(a) maximization of $d_h^{(*)}$;
(b) maximization of $(k_h^{(*)})^2$.

More specifically, we study the following optimization problems:

$$\begin{aligned}
&\text{maximize} : |d_h^{(*)}| \text{ or } (k_h^{(*)})^2 \\
&\text{variables} : \text{volume fraction } f \text{ and element densities } \boldsymbol{x} \\
&\text{subject to} : \text{transversal isotropy of the matrix material} \\
&\text{and} : \text{lower bound constraint on bulk modulus of the matrix } K^{(m)} \\
&\text{and} : \text{lower bound constraint on the volume fraction of piezorods } f. \qquad (19)
\end{aligned}$$

The design procedure consists of the following steps:

(1) take a (porous) matrix material, described by a cubic base cell, discretized by finite elements;
(2) find the effective matrix stiffness properties as a function of the element densities $\boldsymbol{x}$ using the numerical homogenization method and finite-element analysis;

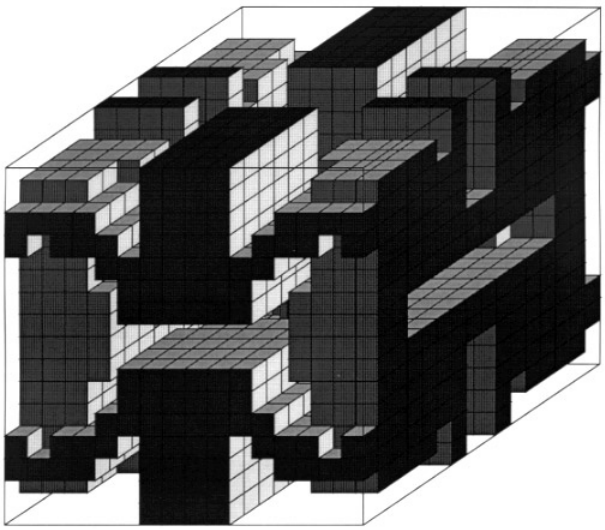

Figure 11. Example a: optimal microstructure (one unit cell) for maximization of the piezoelectric charge coefficient $d_h^{(*)}$.

(3) find the effective piezocomposite properties as functions of the element densities $\boldsymbol{x}$ and the volume fraction of piezoelectric rods f using the aforementioned analytical formulas;
(4) find the hydrophone performance coefficients using the formulas given in [21];
(5) find optimal f by performing golden sectioning loop over steps 3, 4 and 5 until convergence;
(6) perform sensitivity analysis (with respect to density change of each finite element);
(7) change matrix topology (element densities) using linear programming;
(8) go to step 2 (repeat until convergence).

The resulting microstructure topologies are shown in figures 11 and 13, and the resulting hydrophone properties are shown in table 3. In what follows, we will discuss the individual examples and the mechanisms behind the enhanced properties.

4.1.3. Example a: maximization of $d_h^{(*)}$. The resulting optimal microstructure for maximization of the hydrostatic charge coefficient $d_h^{(*)}$ is seen in figure 11.

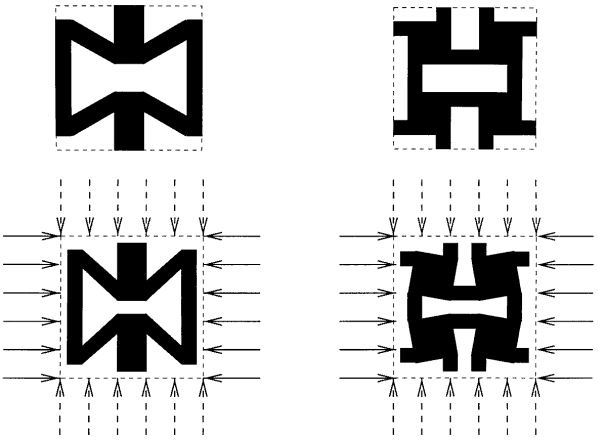

Figure 12. Schematic representation of an equivalent two-dimensional structure that yields the (vertical) negative Poisson's ratio behavior of example a (figure 11). Left: front (1–3 plane) view. Right: side (2–3 plane) view. When the microstructures are compressed horizontally (solid arrows), they contract vertically (dashed arrows).

The resulting effective properties of the matrix material are

$$C^{(m)} = \begin{bmatrix} 0.246 & 0.018 & -0.072 \\ 0.018 & 0.246 & -0.072 \\ -0.072 & -0.072 & 0.216 \end{bmatrix} \times 10^9 \text{ Pa} \qquad (20)$$

or $\nu_{12}^{(m)} = \nu_{21}^{(m)} = -0.027$, $\nu_{13}^{(m)} = -0.27$, $\nu_{31}^{(m)} = -0.34$ and the horizontal and vertical Young's moduli $E_1^{(m)} = 0.23 \times 10^9$ Pa and $E_3^{(m)} = 0.18 \times 10^9$ Pa, respectively. We note that the vertical Poisson's ratio is negative, which means that horizontal forces are inverted and act like compressive forces and result in the enhancement of the hydrostatic charge coefficient. This means that the negative Poisson's ratio of the matrix material makes the effective $d_{13}^{(*)}$-coefficient positive, thus enhancing the overall hydrostatic behavior.

The negative Poisson's ratio behavior of the microstructure in figure 11 can be difficult to imagine. To visualize the mechanism behind the negative Poisson's ratio behavior, we show a two-dimensional interpretation in figure 12. Seen from the front (1–3 plane), the negative Poisson's ratio behavior is seen to resemble the mechanism behind the inverted honeycomb structure [61, 62]. Seen from the side (2–3 plane), the mechanism is seen to be slightly different. Note that the material structure does not need to be hexagonal or fully symmetric to be transversally isotropic (see for example [63] or [33]).

4.1.4. Example b: maximization of $(k_h^{(*)})^2$. The resulting optimal microstructure for maximization of the effective electromechanical coupling factor $(k_h^{(*)})^2$ is seen in figure 13 and an interpretation is seen in figure 14.

The optimal matrix properties for this example are

$$C^{(m)} = \begin{bmatrix} 2.31 & 0.86 & 0.01 \\ 0.86 & 2.31 & 0.01 \\ 0.01 & 0.01 & 0.02 \end{bmatrix} \times 10^9 \text{ N m}^{-2} \qquad (21)$$

or $\nu_{12}^{(m)} = \nu_{21}^{(m)} = 0.37$, $\nu_{13}^{(m)} = 0.003$, $\nu_{31}^{(m)} = 0.32$, $E_1^{(m)} = 2.0 \times 10^9$ Pa and $E_3^{(m)} = 0.02$ Pa.

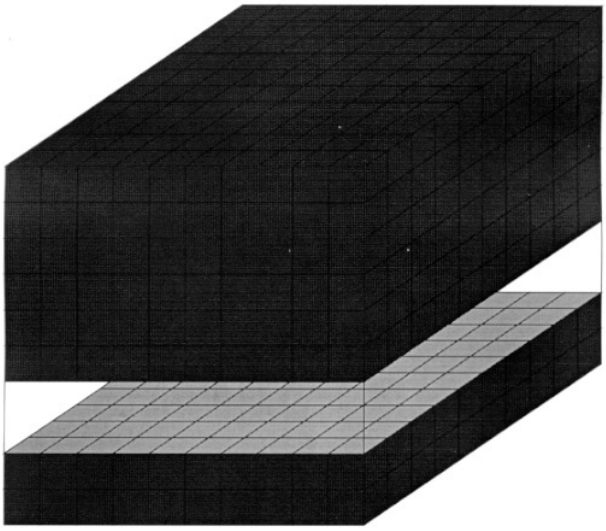

Figure 13. Example b: optimal microstructure (one unit cell) for maximization of the effective electromechanical coupling factor $(k_h^{(*)})^2$.

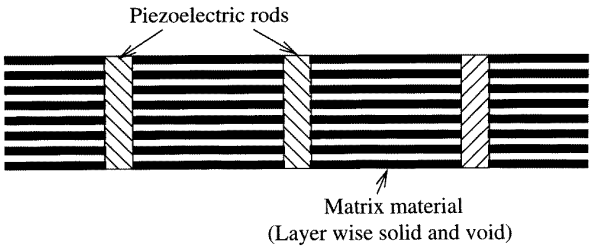

Figure 14. Interpretation (vertical cut) of the piezo-composite design for maximization of $(k_h^{(*)})^2$.

From figure 14, we see that the optimal hydrophone composition is a layered structure of matrix material with embedded piezoelectric rods. The explanation for this is that the optimization procedure tries to decouple the horizontal forces working on $d_{13}^{(*)}$, leading to an overall piezoelectric charge coefficient nearly equal to $d_{33}^{(*)}$.

4.1.5. Manufacturing. A number of different techniques now exist to fabricate our optimal three-dimensional microstructures. We have employed [21] an approach that is based on a stereolithography method developed by 3-D Systems, Inc. [64]. In this method, a laser beam is focused onto a photocurable solution or a dispersion to induce photocuring of an agent in the continuous liquid phase. The desired object is built layer by layer by spreading a thin film, with layer thicknesses between 50 and 200 μm, and then laser curing the film to define a pattern. The layering is repeated multiple times until a desired three dimensional body is completed (figure 15). The two-dimensional sections are created from a three-dimensional solid AutoCAD file and the motion of the laser beam to cure the two-dimensional section is controlled by a computer interpreting the CAD file. Although this method was first developed to fabricate polymeric prototypes, it has now been extended to ceramics with the use of highly concentrated colloidal suspensions [65, 66].

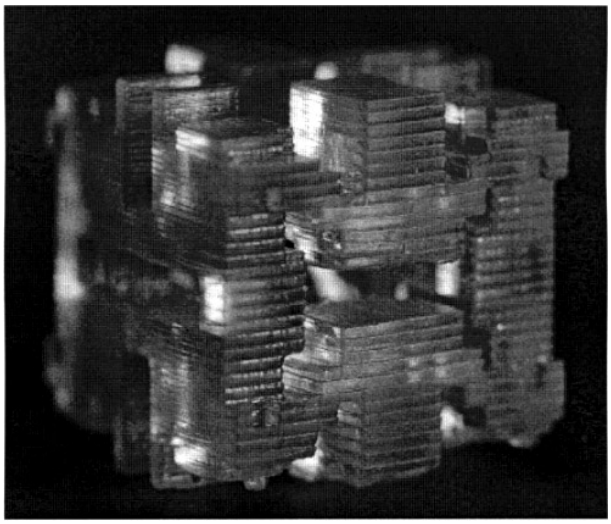

Figure 15. Prototype of one base cell made by stereolithography.

Our approach will be ideal for testing out the optimal models produced by the formalism established in this paper. A prototype [21] consisting of one base cell in larger scale (0.8 cm cubed) for the design in which $d_h^{(*)}$ is maximized (see figure 11) is shown in figure 15. The base cell was produced by the aforementioned manufacturing technique. Recently, we have fabricated a cubic sample consisting of $5 \times 5 \times 5$ cells. We are now in the process of making experimental measurements of the stiffness tensor of this sample matrix material. These data will then be compared against our theoretical predictions of the elastic moduli. Moreover, we will test the performance of the piezocomposite made up of our optimally designed matrices and piezoceramic rods.

5. Conclusions

It is seen that the topology optimization technique (which relies on the finite-element method, homogenization techniques, sensitivity analysis and sequential linear programming) is a very promising means of designing new composite sensors and actuators for smart materials applications. We discussed two applications: design of composites with extreme thermal expansion coefficients and piezocomposites with optimal hydrophone characteristics. In the case of the piezocomposites, we considered fixed topology of the ceramic rods. The next step will be to let the shape of the rods be free to vary as well. This can be done using the three-phase topology method developed in Sigmund and Torquato [33, 34] as discussed in the general section 2. We emphasize that the topology optimization technique also is a useful way to design devices for MEMS applications [28, 29, 19].

Acknowledgments

This work was supported by the ARO/MURI grant DAAH04-95-1-0102 (OS and ST) and Denmark's Technical Research Council (Programme of Research on Computer-Aided Design and Talent-Programme: Topology Optimization Methods for MEMS-Design) (OS).

References

[1] Bendsøe M P and Kikuchi N 1988 Generating optimal topologies in optimal design using a homogenization method *Comput. Methods Appl. Mech. Eng.* **71** 197–224
[2] Cheng K T and Olhoff N 1981 An investigation concerning optimal design of solid elastic plates *Int. J. Solids Struct.* **17** 305–23
[3] Allaire G and Kohn R V 1993 Optimal design for minimum weight and compliance in plane stress using extremal microstructures *Eur. J. Mech.* A **12** 839–78
[4] Bendsøe M P 1995 *Optimization of Structural Topology, Shape and Material* (Springer)
[5] Allaire G, Bonnetier E, Francfort G and Jouve F 1997 Shape optimization by the homogenization method *Numer. Math.* **76** 27–68
[6] Cherkaev A and Palais R 1996 Optimal design of three-dimensional axisymmetric elastic structures **12** 35–45
[7] Diaz A and Lipton R 1997 Optimal material layout for 3D elastic structures *Struct. Optimization* **10** 40–45
[8] Burns T and Cherkaev A 1997 Optimal distribution of multimaterial composites for torsional beams *Struct. Optimization* **13** 4–11
[9] Zhou M and Rozvany G I N 1991 The COC algorithm, part II: topological, geometry and generalized shape optimization *Comput. Methods Appl. Mech. Eng.* **89** 197–224
[10] Bendsøe M P 1989 Optimal shape design as a material distribution problem *Struct. Optimization* **1** 193–202
[11] Mlejnik H P and Schirrmacher R 1993 An engineering approach to optimal material distribution and shape finding *Comput. Methods Appl. Mech. Eng.* **106** 1–26
[12] Ambrosio L and Buttazzo G 1993 An optimal design problem with perimeter penalization *Calc. Var.* **1** 55–69
[13] Haber R B, Bendsøe M P and Jog C 1996 A new approach to variable-topology shape design using a constraint on the perimeter *Struct. Optimization* **11** 1–12
[14] Duysinx P 1997 Layout optimization: a mathematical programming approach *Technical University of Denmark DCAMM Report* 540 submitted
[15] Beckers M 1996 Optimisation topologique de structures continues en variable discretes *University of Liege LTAS Technical Report* OF-38
[16] Beckers M 1997 Methodes du perimetre et des filtres pour l'optimisation topologique en variable discretes *University of Liege LTAS Technical Report* OF-45
[17] Petersson J and Sigmund O 1997 Slope constrained topology optimization *Int. J. Numer. Methods Eng.* **41** 1417–34
[18] Sigmund O 1994 Design of material structures using topology optimization *PhD Thesis* Department of Solid Mechanics, Technical University of Denmark
[19] Sigmund O 1997 On the design of compliant mechanisms using topology optimization *Mech. Struct. Machines* **25** 495–526
[20] Beckers M 1997 Optimisation topologique de structures tridimensionelles en variable discretes *University of Liege LTAS Technical Report* OF-44
[21] Sigmund O, Torquato S and Aksay I A 1997 On the design of 1–3 piezocomposites using topology optimization *J. Mater. Res.* **13** 1038–48
[22] Jog C S 1997 Distributed-parameter optimization and topology design for nonlinear thermoelasticity *Comput. Methods Appl. Mech. Eng.* **132** 117–34
[23] Yuge K and Kikuchi N 1995 Optimization of a frame structure subjected to plastic deformation *Struct. Optimization* **10** 197–208
[24] Swan J S and Arora C C 1997 Topology optimization of material layout in structured composites of high stiffness and strength *Struct. Optimization* **13** 45–59
[25] Yang R J and Chen C J 1996 Stress-based topology optimization *Struct. Optimization* **12** 98–105

[26] Duysinx P and Bendsøe M P 1998 Topology optimization of continuum structures with local stress constraints *Int. J. Numer. Meth. Eng.* **43** 1453–78
[27] Ou J S and Kikuchi N 1996 Integrated optimal structural and vibration control design *Struct. Optimization* **12** 209–16
[28] Ananthasuresh G K, Kota S and Gianchandani Y 1994 A methodical approach to the design of compliant micromechanics *Solid-State Sensor and Actuator Workshop* pp 189–92
[29] Larsen U D, Sigmund O and Bouwstra S 1997 Design and fabrication of compliant mechanisms and material structures with negative Poisson's ratio *J. Microelectromech. Syst.* **6** 99–106
[30] Sigmund O 1994 Materials with prescribed constitutive parameters: an inverse homogenization problem *Int. J. Solids Struct.* **31** 2313–29
[31] Sigmund O 1995 Tailoring materials with prescribed elastic properties *Mech. Mater.* **20** 351–68
[32] Sigmund O 1997 A new class of extremal composites submitted
[33] Sigmund O and Torquato S 1997 Design of materials with extreme thermal expansion using a three-phase topology optimization method *J. Mech. Phys. Solids* **45** 1037–67
[34] Sigmund O and Torquato S 1996 Composites with extremal thermal expansion coefficients *Appl. Phys. Lett.* **69** 3203–5
[35] Silva E C N, Fonseca J S O and Kikuchi N 1997 Optimal design of piezoelectric microstructures *Comput. Mech.* **19** 397–410
[36] Bourgat J F 1997 Numerical experiments of the homogenization method for operators with periodic coefficients *Lecture Notes in Mathematics* (Berlin: Springer) pp 330–56
[37] Guedes J M and Kikuchi N 1991 Preprocessing and postprocessing for materials based on the homogenization method with adaptive finite element methods *Comput. Methods Appl. Mech. Eng.* **83** 143–98
[38] Schultz P C and Smyth K T 1970 Ultra-low-expansion glasses and their structure in SiO_2–TiO_2 system *Amorphous Materials* (New York: Wiley) ch 44, pp 453–62
[39] Kagaya H-M and Soma T 1993 Compression effect on specific heat and thermal expansion of Si and Ge *Solid State Commun.* **85** 617–21
[40] Mary T A, Evans J S O, Vogt T and Sleight W 1996 Negative thermal expansion from 0.3 to 1050 kelvin in ZrW_2O_8 *Science* **272** 90–2
[41] Hausch G, Bächer R and Hartmann J 1989 Influence of thermomechanical treatment on the expansion behavior of Invar and Superinvar *Physica* B **161** 22–4
[42] Baughman R H and Galvão D S 1993 Crystalline networks with unusual predicted mechanical and thermal properties *Nature* **365** 735–7
[43] Newnham R E and Ruchau G R 1991 Smart electro ceramics *J. Am. Ceram. Soc.* **74** 463–80
[44] Smith W A 1991 Optimizing electromechanical coupling in piezo composites using polymers with negative Poisson's ratio *Proc. IEEE Ultrasonics Symp.* (Piscataway, NJ: IEEE)
[45] Christensen R M 1979 *Mechanics of Composite Materials* (New York: Wiley)
[46] Pedersen P 1970 On the minimum mass layout of trusses *Symp. on Structural Optimization (AGARD Conf. Proc. 36)* pp 189–92
[47] Schittkowski K 1994 Numerical comparison of non-linear programming algorithms for structural optimization *Struct. Optimization* **7** 1–19
[48] Hanson R J and Hiebert K L 1981 A sparse linear programming subprogram *Sandia National Laboratories Technical Report* SAND81-0297
[49] Sigmund O and Petersson J 1998 Numerical instabilities in topology optimization dealing with checkerboards, mesh dependencies and local minima *Struct. Optimization* **16** 68–75
[50] Schapery R A 1968 Thermal expansion coefficients of composite materials based on energy principles *J. Composite Mater.* **2** 380–404
[51] Rosen B W and Hashin Z 1970 Effective thermal expansion and specific heat of composite materials *Int. J. Eng. Sci.* **8** 157–73
[52] Gibiansky L V and Torquato S 1997 Thermal expansion of isotropic multi-phase composites and polycrystals *J. Mech. Phys. Solids* at press
[53] Lakes R 1987 Foam structures with negative Poisson's ratio *Science* **235** 1038
[54] ASM 1993 *Properties and Selection (ASM Handbook 2)* (Materials Information Society)
[55] Klicker K A, Biggers J V and Newnham R E 1991 Composites of PZT and epoxy for hydrostatic transducer applications *J. Am. Ceram. Soc.* **64** 5
[56] Ting R Y, Shaulov A A and Smith W A 1992 Evaluation of the properties of 1–3 piezocomposites of a new lead titanate in epoxy resin *Ferroelectrics* **132** 69–77
[57] Newnham R E 1986 Composite electroceramics *Ferroelectrics* **68** 1–32
[58] Chan H L W and Unsworth J 1989 Simple model for piezoelectric ceramic/polymer in ultrasonic applications *IEEE Trans. Ultrason. Ferroelectr. Freq. Control* **36** 434–41
[59] Avellaneda M and Swart P J 1995 Calculating the performance of 1–3 piezocomposites for hydrophone applications: an effective medium approach *Courant Institute of Mathematics Working Paper*
[60] Gibiansky L V and Torquato S 1997 Optimal design of 1–3 composite piezoelectrics *Struct. Optimization* **13** 23–8
[61] Almgren R F 1985 An isotropic three-dimensional structure with Poisson's ratio $= -1$ *J. Elasticity* **12** 839–78
[62] Kolpakov A G 1985 Determination of the average characteristics of elastic frameworks *PMM J. Appl. Math. Mech. USSR* **49** 739–45
[63] Sigmund O 1996 Design and manufacturing of material microstructures and micromechanisms *Proc. 3rd Int. Conf. on Intelligent Material, ICIM96 (Lyon, 1996), SPIE* vol 2779, ed P Gobin (Bellingham, WA: SPIE) pp 856–66
[64] Jacobs P 1992 *Rapid Prototyping and Manufacturing—Fundamentals of Stereolithography* (Dearborn, MI: SME)
[65] Griffith M L and Halloran J W 1996 Freeform fabrication of ceramics via stereolithography *J. Am. Ceram. Soc.* **79** 2601–8
[66] Garg R, Prud'homme R K, Aksay I A, Liu F and Alfano R R 1997 Optical transmission in highly-concentrated dispersions submitted
[67] Garg R 1997 Manufacturing of 3-d microstructures using stereolithography in preparation